LAWRENCE
LIVERMORE
NATIONAL
LABORATORY

LLNL-TR-409956

Surface-pressure Tides Simulated by WACCM-1 and CMIP3 / IPCC Climate Models

Curt Covey, Aiguo Dai, Richard S. Lindzen, Dan Marsh

January 20, 2009

Disclaimer

This work performed under the auspices of the U.S. Department of Energy by Lawrence Livermore National Laboratory under Contract DE-AC52-07NA27344.

Surface-pressure Tides Simulated by WACCM and the CMIP3 / IPCC Climate Models

Curt Covey, Aiguo Dai, Richard S. Lindzen and Dan Marsh
correspondence to: covey1@llnl.gov

16 January 2009

1. Introduction

Atmospheric tides driven by solar heating are readily detectable at Earth's surface as variations in air pressure (Hagan et al. 2003). Above the lower stratosphere (~30 km altitude) the tides attain large amplitudes and can be a significant part of atmospheric motion. Output from the general circulation model (GCM) WACCM, the Whole-Atmosphere Community Climate Model, contains tidal oscillations in its middle and upper atmosphere (Richter et al. 2008, Chang et al. 2008). This result is not surprising since WACCM was designed for middle- and upper-atmospheric research, with its vertical domain extending from the surface to the thermosphere (> 150 km altitude). However, WACCM output has not previously been examined for the surface signature of the tides. We do so in this report for both the original version (WACCM-1; Sassi et al. 2002) and the latest version (WACCM-3; Richter et al. 2008) of the model.

We also search for atmospheric tides in output from the climate models contributing to the latest assessment report of the Intergovernmental Panel on Climate Change, or IPCC (Randall et al. 2007). Output from models of this type has been examined for tides in only a few cases (Dai and Trenberth 2004, Woolnough et al. 2004). Climate modelers designing coupled ocean-atmosphere GCMs generally do not have atmospheric tides or the middle atmosphere in mind during the model development process. Indeed, many climate-oriented GCMs extend upward to only ~30-40 km altitude.

We compare model-simulated tides with the most recent and complete set of surface pressure observations (Dai and Wang 1999). We focus our attention on surface pressure because this variable is the most readily available in both the IPCC model output and the observations.

The theme of our investigation is the role of the middle and upper atmosphere (i.e. above ~10 km altitude) in producing surface pressure tides. Classical linear theory implies a major role for stratospheric ozone heating in forcing the semidiurnal (twice a day) tide component at the surface, and it explains why the semidiurnal component dominates the observed tides (Chapman and Lindzen 1970). One might therefore expect that models with tops below the ozone heating peak (~50 km altitude) or with poor resolution in the middle atmosphere would produce surface pressure tides that are weaker than observed and perhaps dominated by the diurnal (once a day) component. In fact, our preliminary analysis reveals no such correlation between model features and the quality of tide simulation. Even GCMs that include only half the stratosphere produce reasonable diurnal *and* semidiurnal surface pressure tides! Of course a complex mathematical model

like a GCM can produce "the right answer for the wrong reasons." One possibility is discussed briefly below and will be the subject of future investigation.

2. Data Sources

All of the model output we analyze is publicly available. WACCM output from the early version of the model (WACCM-1; Sassi et al. 2002) was downloaded from NCAR's Community Data Portal (http://cdp.ucar.edu). WACCM output from the latest version of the model (WACCM-3; Richter et al. 2008) was provided by the WACCM Working Group of the Community Climate System Model (CCSM). Membership in this and other CCSM Working Groups is open to any interested scientist (see http://www.ccsm.ucar.edu/working_groups/WACCM). The IPCC output was taken from archives of the Coupled Model Intercomparison Project, phase 3 (CMIP3; see Meehl et al. 2007) on the PCMDI's Earth System Grid portal (http://esg.llnl.gov/portal). We downloaded the model output in late 2007 and 2008.

WACCM was driven by observed sea surface temperature and sea ice concentration as lower boundary conditions. All IPCC models were driven by incoming solar energy flux at the top of the atmosphere together with observed greenhouse gas and aerosol concentrations; they calculated ocean temperature and sea ice interactively (i.e. as part of a coupled ocean-atmosphere GCM). In addition, some IPCC atmospheric GCMs were driven by observed sea surface temperature and sea ice concentration as lower boundary conditions. We demonstrate below that these different types of boundary condition make no significant difference to the simulation of atmospheric surface-pressure tides.

3. Results from WACCM

The starting point for global analysis of WACCM output is 3-hourly surface pressure data, expressed for each day and grid point as anomalies relative to that day's and grid point's mean value. Fourier analysis in the time dimension was done by postprocessing WACCM-1 output and by inline-computing during WACCM-3 simulation. The results show that the dominant frequency of surface-pressure tides is semidiurnal rather than diurnal—in both the observations and the model—over most of the globe. Exceptions to semidiurnal dominance occur in land areas at lower latitudes, where heat flux from the surface induces large diurnal variations in both observations and the model (Figure 1). The observations also show a significant diurnal tide in mid-latitude elevated terrain (the Andes, the Rockies, Tibetan Plateau). The WACCM simulations do not reproduce this feature of the tides. In both model and observations, the semidiurnal tide's amplitude is substantially larger than the diurnal amplitude in the global mean, and it decreases from the tropics to higher latitudes (Figure 2). For the diurnal tide, WACCM-1 overestimates amplitude by a factor > 2 over tropical land, including the "maritime continent" of Indonesia, while underestimating it by about one-third globally; WACCM-3 corrects the overestimate but not the underestimate. For the semidiurnal tide amplitude, an overestimate (by ~20%) in lower latitudes and an underestimate in higher latitudes is produced by both versions of WACCM.

The phase of the tides equatorward of 28° North and South latitude, where amplitudes are significant, puts the diurnal pressure maximum around 6 AM local solar time (Figure 3) and the semidiurnal pressure maximum around 10 AM and PM local solar time (Figure 4) in both the model and observations. Thus the model correctly simulates both the dominance and timing of the semidiurnal component at low latitudes, where its amplitude is largest. It is apparent from Figures 3-4, however, that the model-simulated phase of both the diurnal and semidiurnal tides is more spatially uniform than indicated by the observations. The noisy observed phase patterns at high latitudes, however, are mainly due to the large errors in estimating phases of the weak tidal cycles there. Also, substantial sampling errors occur over the southern ocean and polar regions; these sampling errors probably have contributed to the regional variations of phase in the observations. Furthermore, at all latitudes it is difficult to interpolate observed phase because estimates from station data can vary considerably between neighboring stations (Dai and Wang 1999). Observed and model-simulated tidal phases at one latitude-longitude point are compared below (see Table 1).

More precise information about the speed and direction of tide propagation comes from an additional Fourier analysis in the longitude (zonal) dimension. This analysis produces tidal amplitude as a function of latitude and zonal wavenumber s, given tidal amplitude as a function of latitude and longitude. Using the algorithms of Dai and Wang (1999), we obtain the results shown in the top two panels of Figures 5 and 6 for the diurnal and semidiurnal components, respectively, of WACCM's simulation. The corresponding observations (same data as shown in Dai and Wang's Figures 7 and 14) are displayed in the bottom panels of our Figures 5 and 6.

Qualitative agreement of simulation and observation is apparent in Figures 5 and 6. They show that where tidal amplitude is significant (equatorward of ~45° North and South latitude) it is concentrated at $s = 1$ for the diurnal tide and $s = 2$ for the semidiurnal tide, in both model output and observations. By definition, tidal variations are proportional to $\exp[i (s \lambda + 2\pi n t / T)]$ where λ = east longitude, t = time, T = 24 hours, $n = 1$ for the diurnal tide, and $n = 2$ for the semidiurnal tide. Thus Figures 5 and 6 show that $s = n$ for the principal parts of both the diurnal and semidiurnal tides, implying that they migrate westward in step with the apparent motion of the Sun across the sky.

Quantitative comparison, however, reveals that WACCM puts too much amplitude into the migrating ($s = n$) components and too little amplitude into the non-migrating ($s \neq n$) components. For the semidiurnal harmonic (Figure 6) the peak model-simulated migrating tide is about 140 Pa, twice the observed value.

In sum, while the observations undoubtedly contain some artificial spatial variations as a result of sampling errors, it is clear from Figures 1-2 and 5-6 that the model misses robust observed features of the tides, most notably the large diurnal variations over mid-latitude high terrain and the non-migrating component of the tides. Evidently the model does not faithfully represent some physical processes that enhance the non-migrating tides, e.g. strong sensible heating of high terrain and zonal variations of tropical heating.

4. Results from the IPCC Climate Models

We now consider the CMIP3 / IPCC model output. Nine contributions to the CMIP3 database included high-frequency (3-hourly) output of *sea-level* pressure from coupled ocean-atmosphere simulations of the 20th century. Unfortunately, the database does not contain high-frequency output of *surface* pressure. The two are of course identical for ocean areas but can differ significantly over land.

Six of the nine models also provided high-frequency output of a single year (2000) from atmosphere-only simulations using observed sea surface temperatures and sea ice concentrations (i.e., AMIP simulations). At the time we extracted the data (2007-2008) three of the models had a simple error in the time-coordinate values recorded for CMIP3. After consulting the model developers, we added 1.5 hours to GISS-EH and GISS-ER times, and we subtracted 4.5 hours from INM-CM3.0 times, to correct these errors.

Table 1 shows our first screening test of the CMIP3 / IPCC output, including a comparison with both sea-level and surface pressure output from WACCM-1. We took an area average in the vicinity of Batavia (now Jakarta), Indonesia, from both the models and observations. The classic signature of the tides—shown for example in Figure 1.1 of Chapman and Lindzen (1970)—is a semidiurnal variation of surface pressure at this location. Chapman and Lindzen's figure shows data taken at Batavia during the first half of November 1919; the amplitude is ~100 Pa and the phase puts maxima at about 10 AM and 10 PM Local Solar Time. Dai and Wang's analysis of observations confirms that the "Batavia" measurements are representative of the tropics in all seasons (Dai and Wang 1999; also see Figures 2 and 4).

From Table 1, we see that all of the models obtain roughly the correct diurnal and semidiurnal amplitudes and phases at Batavia. Comparing results from the coupled ocean-atmosphere 20th century simulations with results from the AMIP simulations shows close agreement. For each model that provided an AMIP simulation, the difference between it and the coupled ocean-atmosphere simulation is 10% or less in amplitude, and 17 minutes or less in phase, for the dominant semidiurnal component of the tide. We conclude that the tide simulations are not sensitive to errors in SST and sea ice amounts, or to chaotic "weather" effects. Note also that diurnal variations of SST are not included in the AMIP boundary conditions (which use monthly-mean SST forcing) so that Table 1 also implies that diurnal variations of SST do not play an important role in the surface pressure tides.

As with WACCM, our starting point for global analysis of CMIP3 / IPCC model output is the complete set of available 3-hourly pressure data, expressed for each day and grid point as anomalies about that day's and grid point's mean value. The GISS and MIROC3.2 medium-resolution models provided 10 simulated years of 3-hourly data, GFDL-CM2.0 provided 5 years, MIROC3.2 high-resolution provided 2 years, and all others provided 1 year. As a preliminary test, we examined the final two days of each time series. Animations (not shown) clearly reveal low-latitude wavenumber-2

disturbances propagating westward with the Sun's apparent motion across the sky. Figure 7 shows one time point from each model's animation. The time point is 9 AM GMT except for the INM-CM3.0 map, which is at 10:30 AM GMT. The time-recording problem noted above for INM-CM3.0 resulted in no data available for 9 AM or PM GMT.

All of the "snapshots" in Figure 7 exhibit a low-latitude wavenumber-2 disturbance maximizing at around 10 AM and PM local solar time, in agreement with the observations (cf. Figure 2 of Dai and Wang 1999, and Figure 4 of Dai and Trenberth 2004). Because the maps in Figure 7 are differences between instantaneous snapshots and corresponding daily means, they also show residuals of baroclinic waves at middle latitudes.

5. Discussion

The resemblance of the maps in Figure 7 to each other—and to the observations—is at first sight surprising. The CMIP3 / IPCC models were designed to simulate large-scale weather patterns and global climate change, not atmospheric tides. One might think that since the tides are a linear response to known forcing, simulation of them would happen automatically in a comprehensive GCM, but it was not clear to us at the outset of this project that the CMIP3 / IPCC models included all of the relevant forcing or the ability to transmit it to the surface. The models differ not only in horizontal resolution (apparent in the smoothness or lack of it in Figure 7's maps) but also in vertical domain and resolution, as noted in the Table 1. Two of the models have "tops" at about the 10 mbar pressure level (~30 km altitude), omitting much of the stratosphere. Among the other models, the number of levels in the stratosphere ranges from 4 to 22. Classical tidal theory (Chapman and Lindzen 1970) and current opinion has at least half of the surface-pressure tide forced by stratospheric ozone heating. Downward gravity wave propagation carries the tide to the surface; this propagation is more efficient for the semidiurnal than the diurnal harmonic of the ozone forcing. The remainder of the semidiurnal tide forcing, and most of the diurnal tide forcing, arises in the lower atmosphere from solar energy absorption by water vapor and from latent heat release associated with daily variation in convective rainfall.

These considerations might lead one to expect the CMIP3 / IPCC models with tops at ~10 mbar to omit much of semidiurnal tide forcing, and the models with poorer stratospheric resolution to have more difficulty propagating it to the surface. Indeed, examination of model-input ozone at altitudes below the 10-mbar pressure level reveals that all of the models use the same mixing ratios (not shown; note also that the CMIP3 database does not include radiative heating or ozone amounts for $p < 10$ mbar). Thus, the two models with a top at 10 mbar do not artificially compensate for their missing ozone heating by increasing it at lower levels. Nevertheless these models—and the ones with a stratosphere represented only at crude vertical resolution—appear to simulate surface-pressure tides with comparable fidelity to models with a more complete middle atmosphere, including WACCM.

To explain this surprising situation, it may be helpful to recall that complex mathematical models can produce subtle "canceling errors" that lead to "the right answer for the wrong reasons." This has happened from time to time in the history of GCM development. For example, implementation of a more accurate finite-volume numerical method in the Community Atmosphere Model (CAM) degraded coupled ocean-atmosphere simulation of climate near Greenland. It was subsequently discovered that ocean heat mixing in this region was inappropriately parameterized in the ocean GCM linked to CAM. When this problem was fixed, and at the same time the more accurate numerics were implemented in CAM, the climate simulation became acceptable again (Neale 2007). In retrospect, the previous model configuration could be described as including two errors—one in the atmosphere and one in the ocean—that partially canceled each other to produce a more accurate climate simulation.

An analogous "canceling error" situation may arise in GCM simulations of atmospheric tides (Lindzen et al. 1968). A model top at 10 mbar could artificially reflect upward-propagating gravity waves downward, spuriously enhancing the semidiurnal tide at the surface and thereby making up for the lack of ozone forcing at altitudes above the 10-mbar pressure level. It would be pure speculation at this point, however, to attribute this feature to any of the models considered here. A possible step toward resolving the issue would employ classical (linear) tide calculations with the geometries and forcing factors pertinent to the various GCMs examined in the present study.

Separately, we are extending our analysis of surface-pressure tides in the CMIP3 / IPCC models. Here we must confront the limitation noted above in the CMIP3 database: the high-time-frequency data include sea level pressure rather than surface pressure. In future work we will attempt to reconstruct high-frequency surface pressure from high-frequency sea level pressure.

Acknowledgements: We thank the Community Climate System Model's WACCM Working Group for valuable advice, and Sabrina Fletcher for graphic art. This work was performed in part under auspices of the Office of Science, U. S. Department of Energy, by the Lawrence Livermore National Laboratory under Contract DE-AC52-07NA27344.

REFERENCES

Chapman, S., and R. S. Lindzen, 1970: Atmospheric Tides, D. Reidel, 200 pp.

Chang, L., S. Palo, M. Hagan, J. Richter, R. Garcia, D. Riggin and D. Fritts, 2008: Structure of the Migrating Diurnal Tide in the Whole Atmosphere Community Climate Model (WACCM), Advances in Space Research 41: 1398-1407

Dai, A., and J. Wang, 1999: Diurnal and Semidiurnal Tides in Global Surface Pressure Fields, Journal of the Atmospheric Sciences, 56, 3874-3890

Dai, A., and K. E. Trenberth, 2004: The Diurnal Cycle and its Depiction in the Community Climate System Model, Journal of Climate, 17, 930-951

Hagan, M. E., J. M. Forbes and A. Richmond, 2003: Atmospheric Tides, in the Encyclopedia of Atmospheric Sciences, ed. J. R. Holton, Academic Press

Lindzen, R.S., E.S. Batten and J.-W. Kim, 1968: Oscillations in atmospheres with tops, Monthly Weather Review 96: 133-140

Meehl, G.A, C. Covey, T. Delworth, M. Latif, B. McAvaney, J.F.B. Mitchell, R.J. Stouffer and K.E. Taylor, 2007: The WCRP CMIP3 multimodel dataset: A new era in climate change research, Bulletin of the American Meteorological Society, September 2007 issue, pp. 1383-1394

Neale, R., 2007: Overview of CAM and CCSM results with three configurations, presentation at the CCSM Atmospheric Model Working Group meeting, Boulder, CO, 29 January 2007 (available on the Web at http://www.ccsm.ucar.edu/csm/working_groups/Atmosphere/Presentations/amwgmeeting2006Jan/Neale_amwg07.ppt)

Randall, D.A., R.A. Wood, S. Bony, R. Colman, T. Fichefet, J. Fyfe, V. Kattsov, A. Pitman, J. Shukla, J. Srinivasan, R.J. Stouffer, A. Sumi and K.E. Taylor, 2007: Climate Models and Their Evaluation. In: Climate Change 2007: The Physical Science Basis. Contribution of Working Group I to the Fourth Assessment Report of the Intergovernmental Panel on Climate Change [Solomon, S., D. Qin, M. Manning, Z. Chen, M. Marquis, K.B. Averyt, M.Tignor and H.L. Miller (eds.)]. Cambridge University Press, Cambridge, United Kingdom and New York, NY, USA

Richter, J., F. Sassi, R.R. Garcia, K. Matthes, and C.A. Fischer, 2008: Dynamics of the middle atmosphere as simulated by the Whole Atmosphere Community Climate Model, version 3 (WACCM3), Journal of Geophysical Research 113, D08101, doi: 10.1029/2007JD009269

Sassi, F.S., R.R. Garcia, B.A. Boville, and H. Liu, 2002: On temperature inversions and the mesospheric surf zone, Journal of Geophysical Research 107 (D19), 4380, doi: 10.1029/2001JD001525

Woolnough, S.J., J.M. Slingo and B.J. Hoskins, 2004: The diurnal cycle of convection and atmospheric tides in an aquaplanet GCM, Journal of the Atmospheric Sciences 61: 2559-2573

TABLE 1: Tides Near "Batavia" (now Jakarta): 14°S-2°N, 97.5°E-112.5°E

Source*			Diurnal component		Semidiurnal component	
	Top of model	Str+ levs**	Amplitude [mbar]	Time of max [LST]	Amplitude [mbar]	Time of max [LST]
CNRM-CM3	0.05 mb	20	0.7165	4:35	1.4010	9:35
CNRM-CM3 AMIP			0.7601	4:42	1.3762	9:38
GFDL-CM2.0	3.00 mb	4	0.4402	6:16	1.3455	10:22
GFDL-CM2.1	3.00 mb	4	0.6095	5:46	1.3112	10:39
GISS-EH	0.10 mb	10	0.7039	4:15	1.7625	10:35
GISS-ER	0.10 mb	10	0.9469	4:19	1.8195	10:33
GISS-ER AMIP			0.7762	4:54	1.7533	10:09
INM-CM3.0	10.00 mb	7	0.6513	5:08	1.4486	10:04
INM-CM3.0 AMIP			0.7378	3:47	1.4763	10:03
MIROC3.2(hi-res)	40 km	22	0.4043	6:16	1.4801	10:09
MIROC3.2(hi-res) AMIP	≈ 3 mb		0.5774	6:31	1.4452	10:11
MIROC3.2(med-res)	30 km	6	0.6403	6:60	1.7809	10:54
MIROC3.2(med-res)AMIP	≈ 10 mb		0.6238	7:34	1.6323	10:52
MRI-CGCM3.2	0.40 mb	7	0.5923	5:46	1.9330	11:14
MRI-CGCM3.2 AMIP			0.4899	5:38	1.7558	10:57
WACCM-1 Jan climat PS			0.5205	5:17	1.2520	10:48
WACCM-1 Jan climat PSL	3×10^{-6}	51	0.5491	5:12	1.2599	10:48
WACCM-1 Jul climat PS	mb		0.5709	3:15	1.1361	10:48
WACCM-1 Jul climat PSL			0.5945	3:17	1.1428	10:47
WACCM-3 Jan climat PS	3×10^{-6}mb	51	0.5474	4:34	1.3474	9:53
OBSERVATIONS			0.6491	5:59	0.9984	9:56

*Observations are from Dai and Wang (1999) for the September – October – November season of years 1976-1997. CMIP3 / IPCC AR4 model results are for the first half of November, corresponding to the "classic" observation described in the text, during the first year of high-frequency model output (1991 for all CMIP3 models except INM-CM3.0, in which the first year is 2000). All models are coupled atmosphere – land surface – ocean – sea ice GCMs with realistic late-20th century forcing (time-varying greenhouse gas and aerosol amounts, time-varying solar energy input, etc.) except for sources labeled "AMIP" or "climat." AMIP simulations force an atmospheric GCM with sea surface temperatures and sea ice concentrations observed for the period 1979 – present; climatology runs force with a repeating climatological-average seasonal cycle of SST and sea ice. Shaded and unshaded rows are used to distinguish different atmospheric GCMs. For CMIP3 model information, see Table 8.1 in Randall et al. (2007) and references therein. Observations are of surface pressure. Model output is sea-level pressure from CMIP3, both sea-level pressure (PSL) and surface pressure (PS) from WACCM-1, and surface pressure from WACCM-3. WACCM-1 output is from a one-year control run; WACCM-3 output is from an arbitrarily selected year (nominally 1991) of a 30-year control run.

**Number of model levels in or above the stratosphere, defined here as altitudes > 15 km or pressure-levels < 150 mbar.

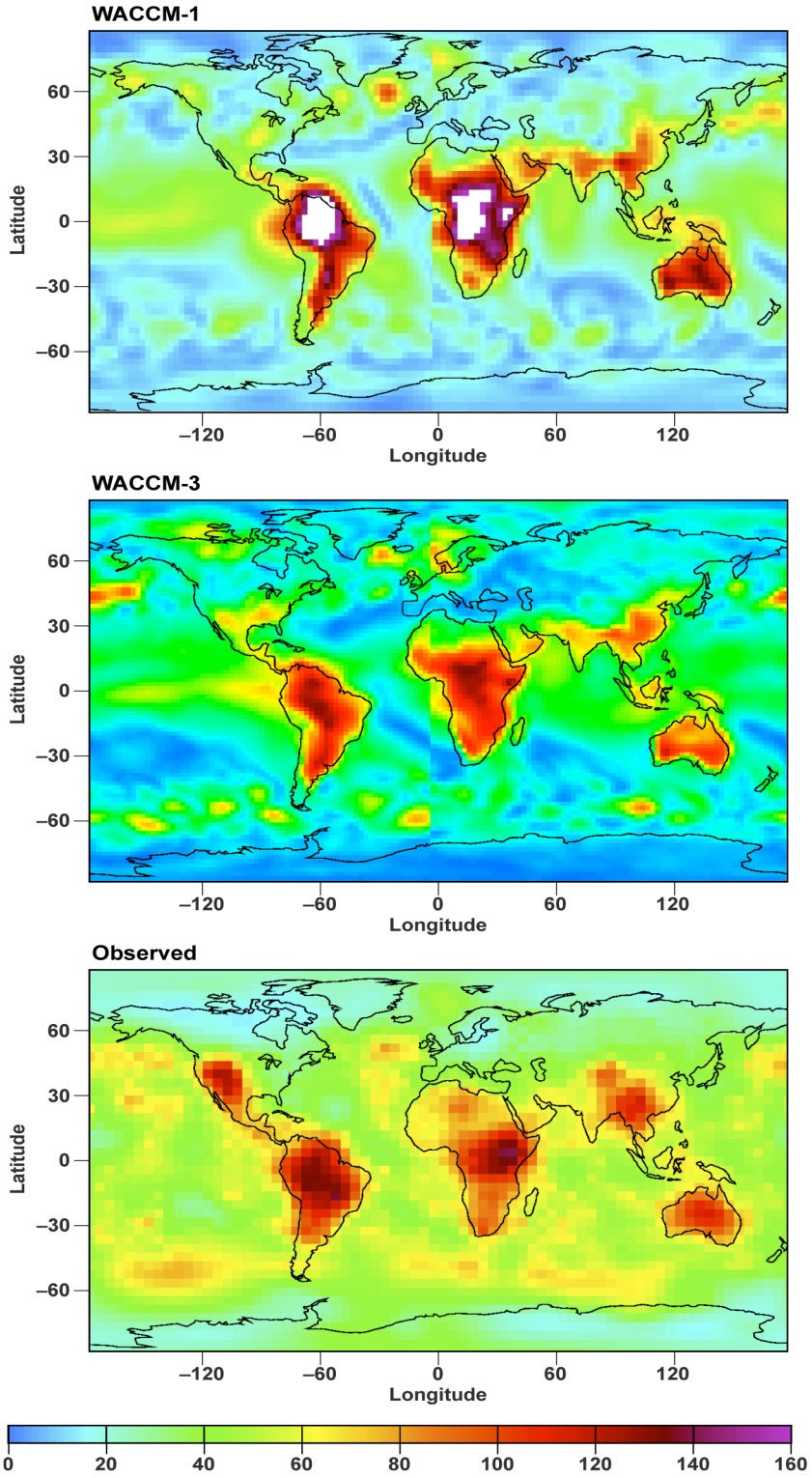

FIGURE 1: Amplitude in Pascals of the diurnal (24 hour) cycle in January surface pressure from a one-year WACCM control run (*top*), January 1991 surface pressure from a multi-year WACCM-3 control run (*middle*), and December – January – February surface pressure observed during 1976-1997 (Dai and Wang 1999) (*bottom*). White areas are off the high end of the color scale and reach a maximum of 215 Pa.

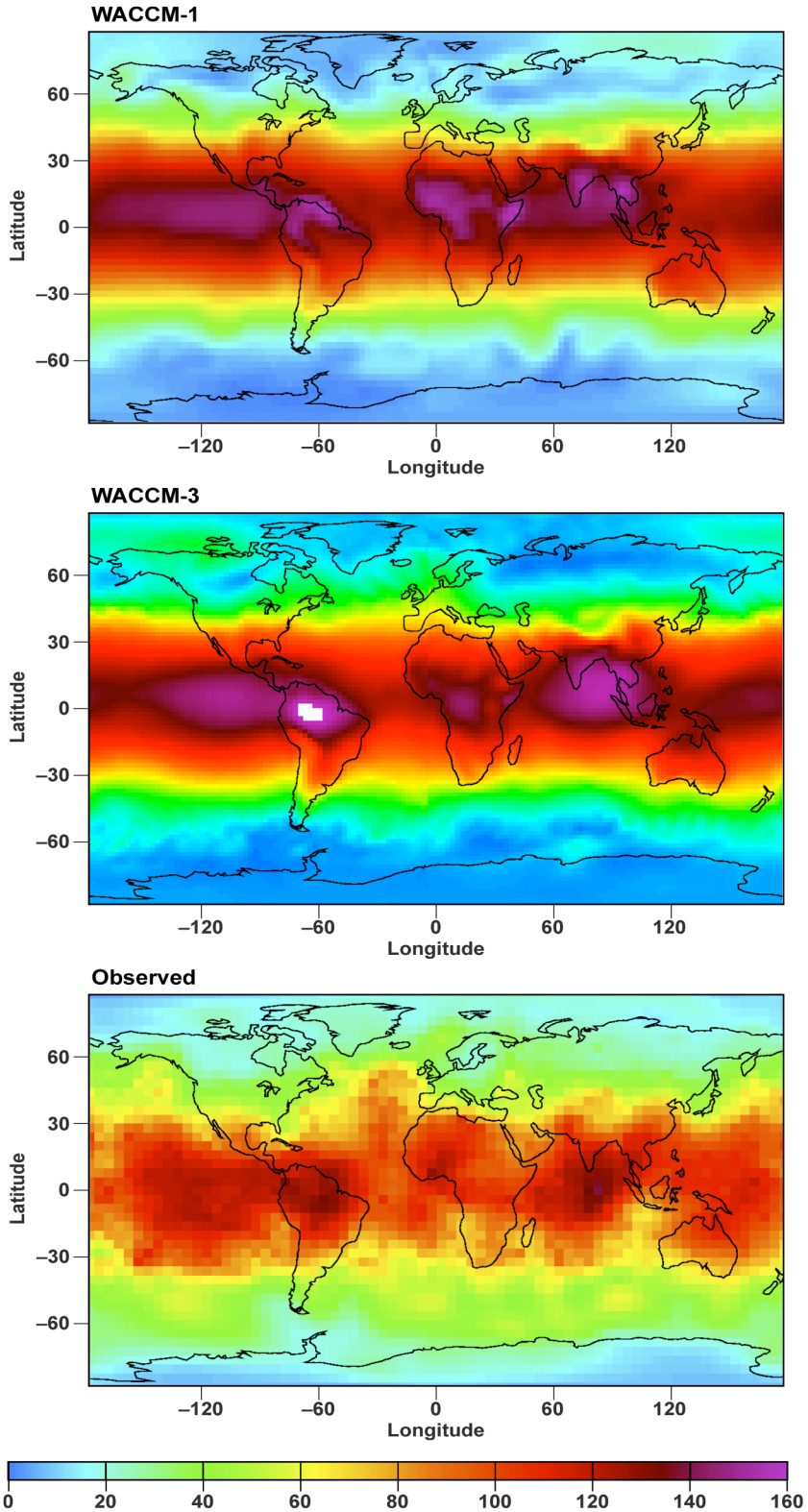

FIGURE 2: Same as Figure 1 for the semidiurnal (12 hour) amplitude. In this case the white areas are only slightly off-scale, reaching a maximum of 163 Pa.

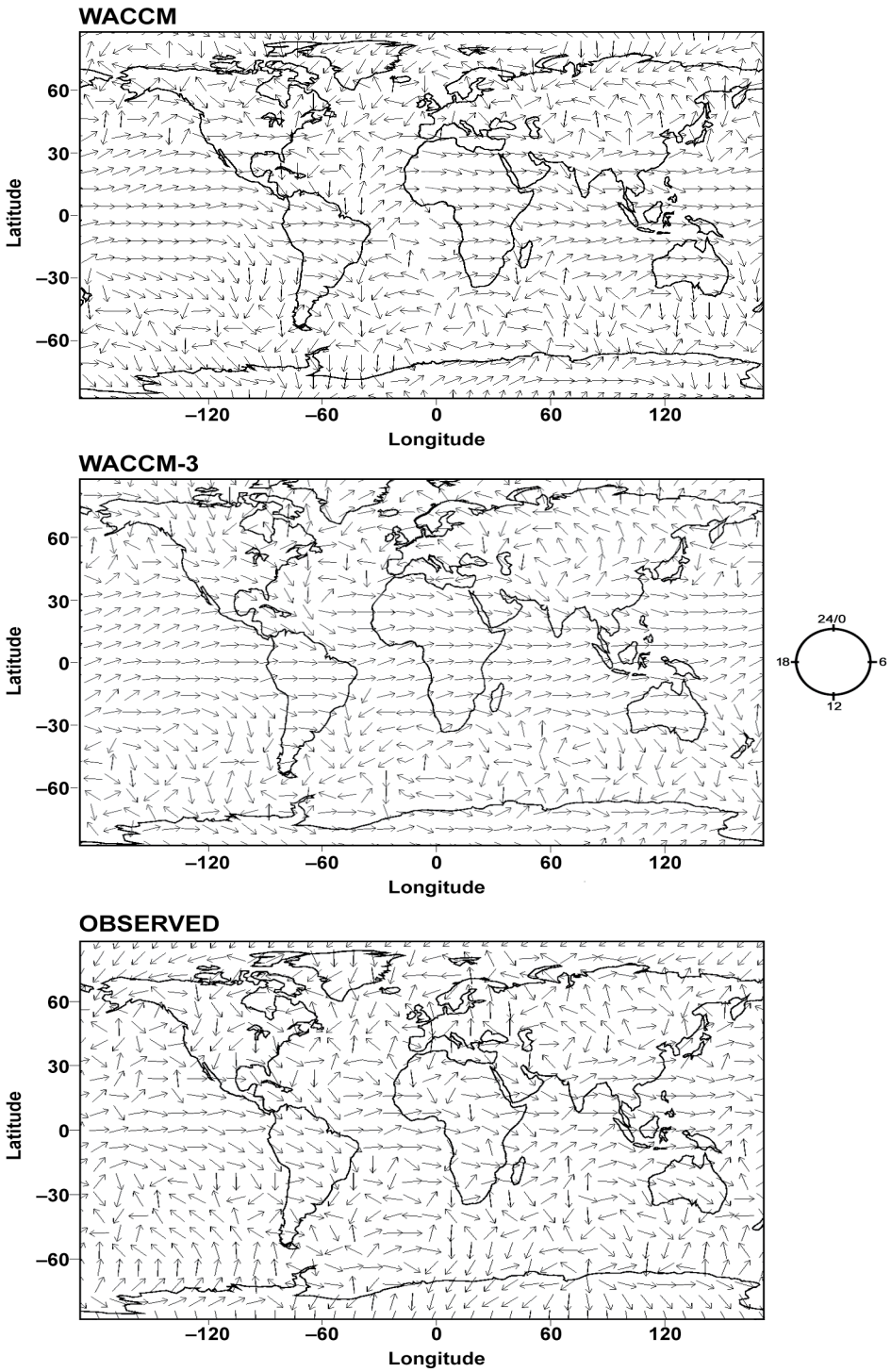

FIGURE 3: Local solar time (in hours) of the maximum of the diurnal surface-pressure tide in January from the WACCM-1 control run (*top*), in January 1991 from the WACCM-3 control run (*middle*), and in December – January – February observations during 1976-1997 (Dai and Wang 1999) (*bottom*).

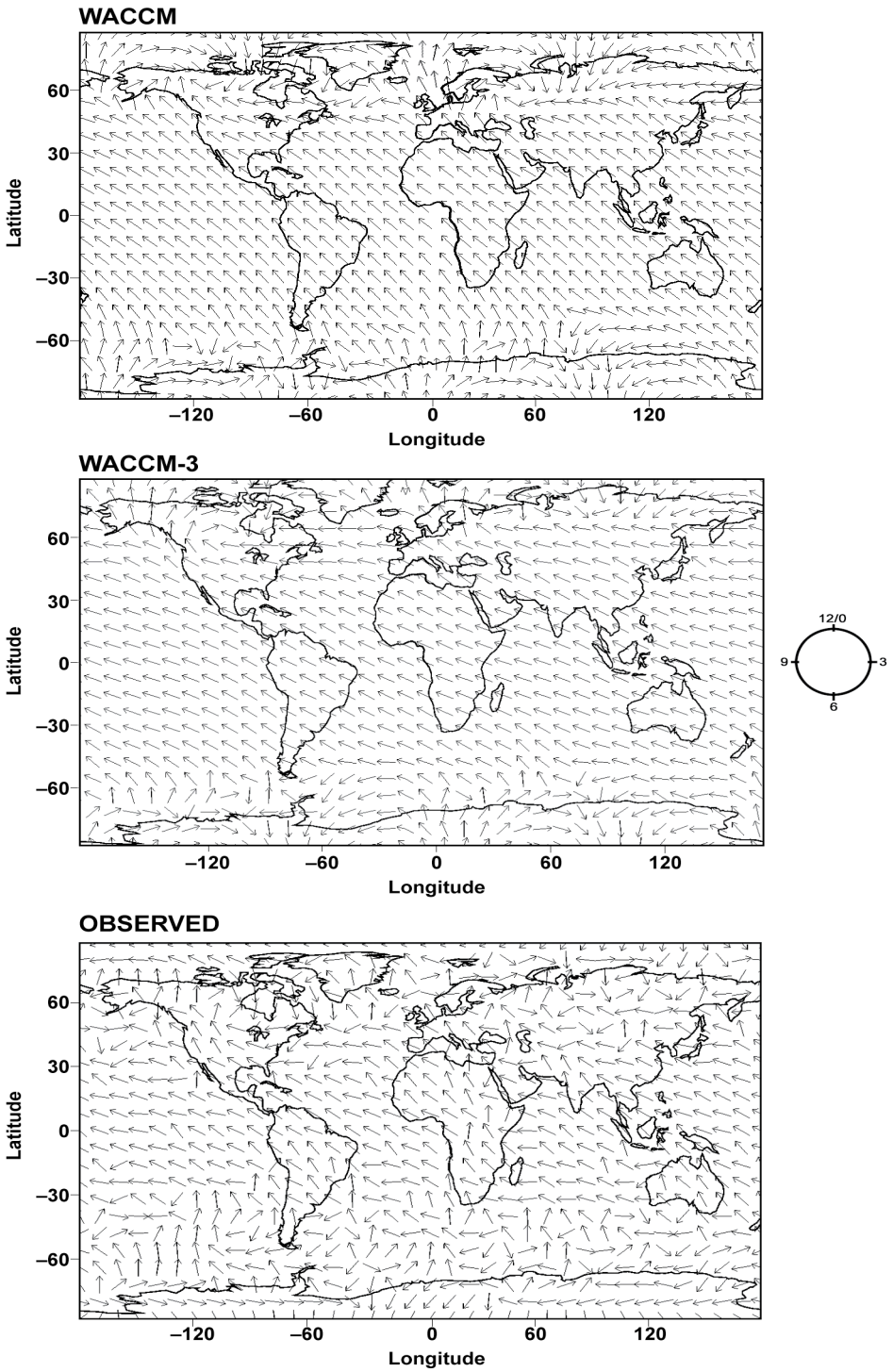

FIGURE 4: Same as Figure 3 for the semidiurnal (12 hour) phase. Note that the clock-face goes from 0 to 12 (rather than 24) hours.

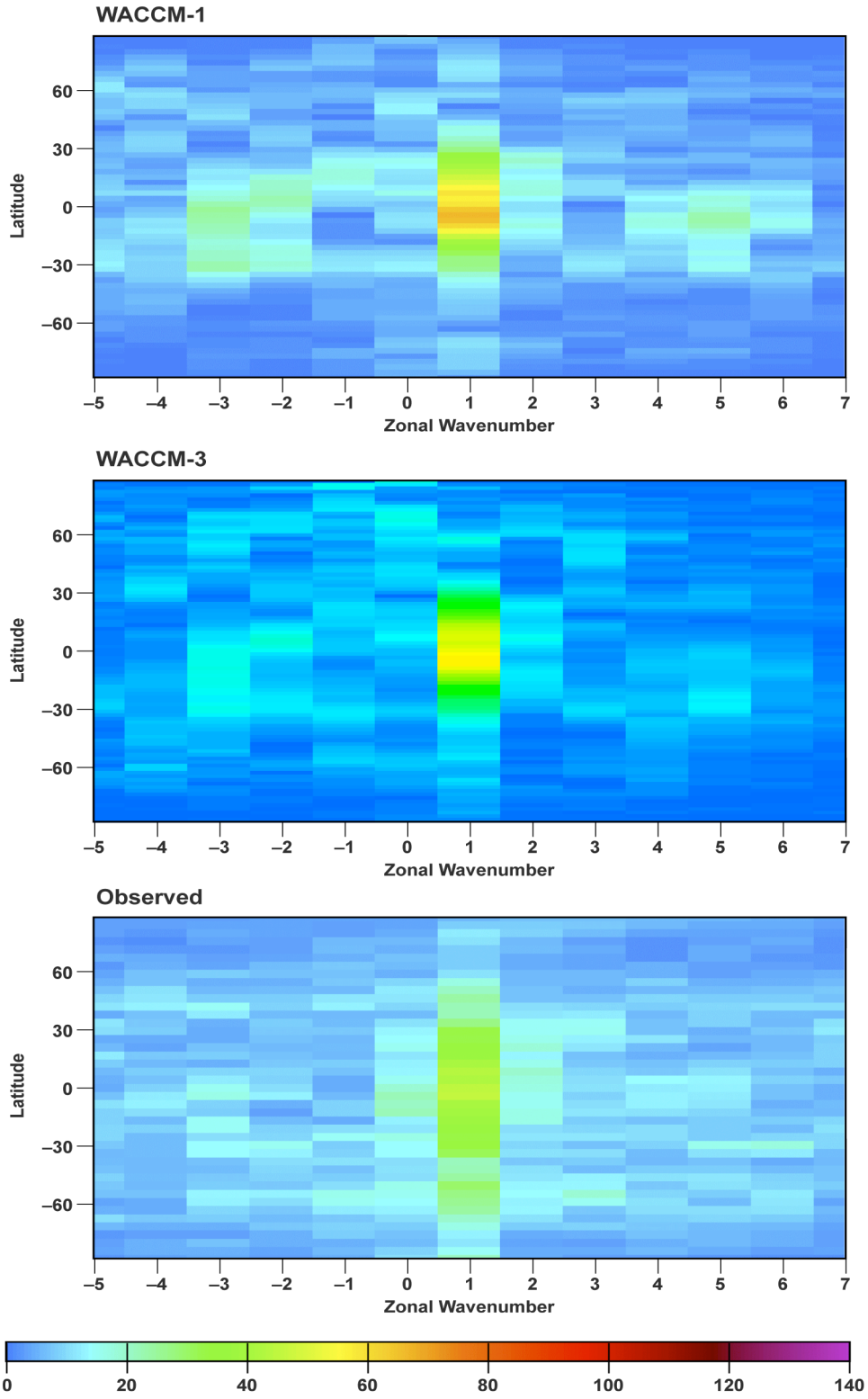

FIGURE 5: Latitudinal distribution of the amplitude (in Pascals) of the diurnal surface-pressure tide as a function of zonal wavenumber in January from the WACCM-1 control run (*top*), in January 1991 from the WACCM-3 control run (*middle*), and in December – January – February observations during 1976-1997 (Dai and Wang 1999) (*bottom*).

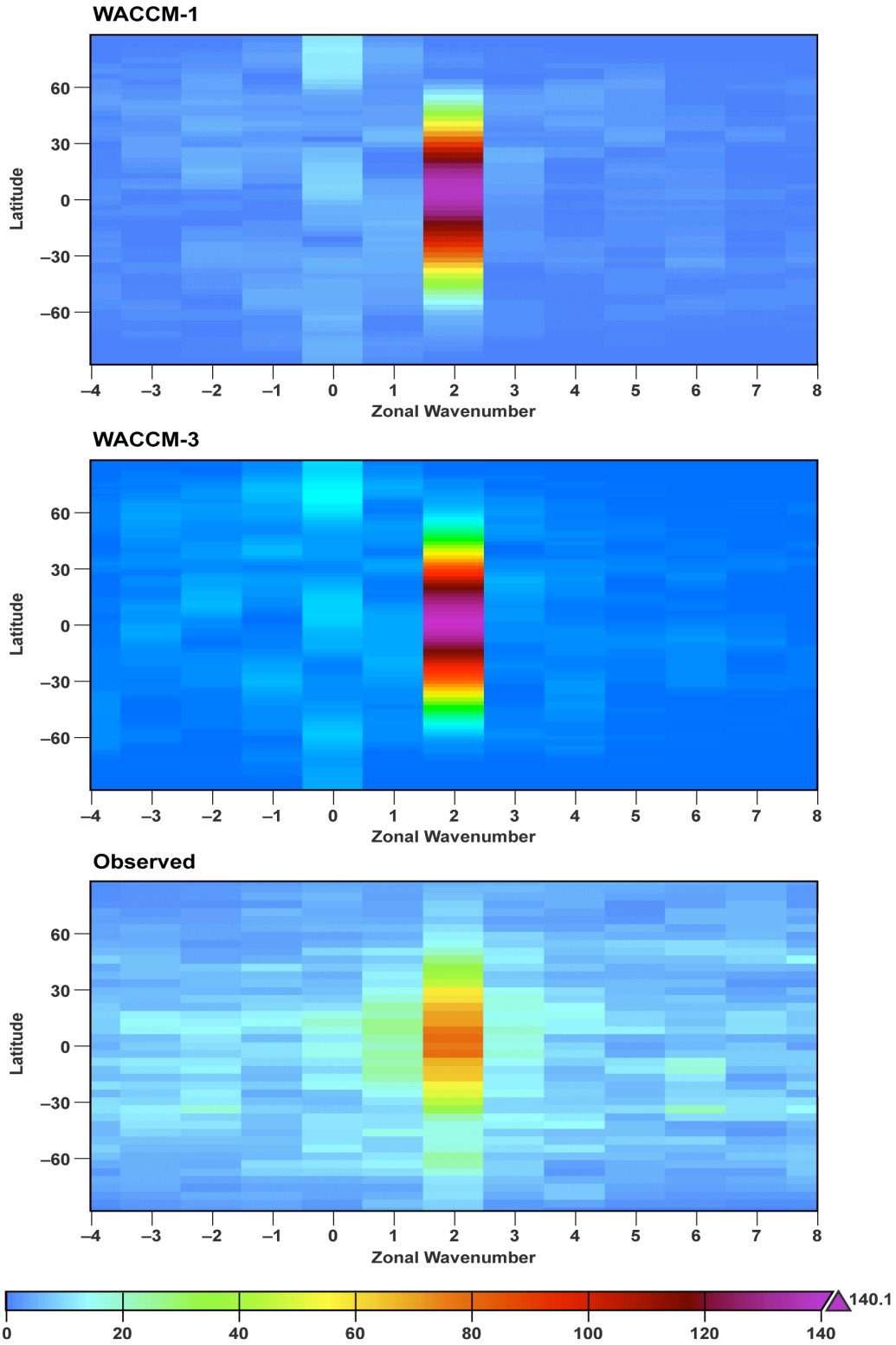

FIGURE 6: Same as Figure 5 for the semidiurnal tide. As indicated in the color bar, the maximum value (for Wavenumber 2 on the Equator in the WACCM-3 simulation) is slightly greater than 140 Pa.

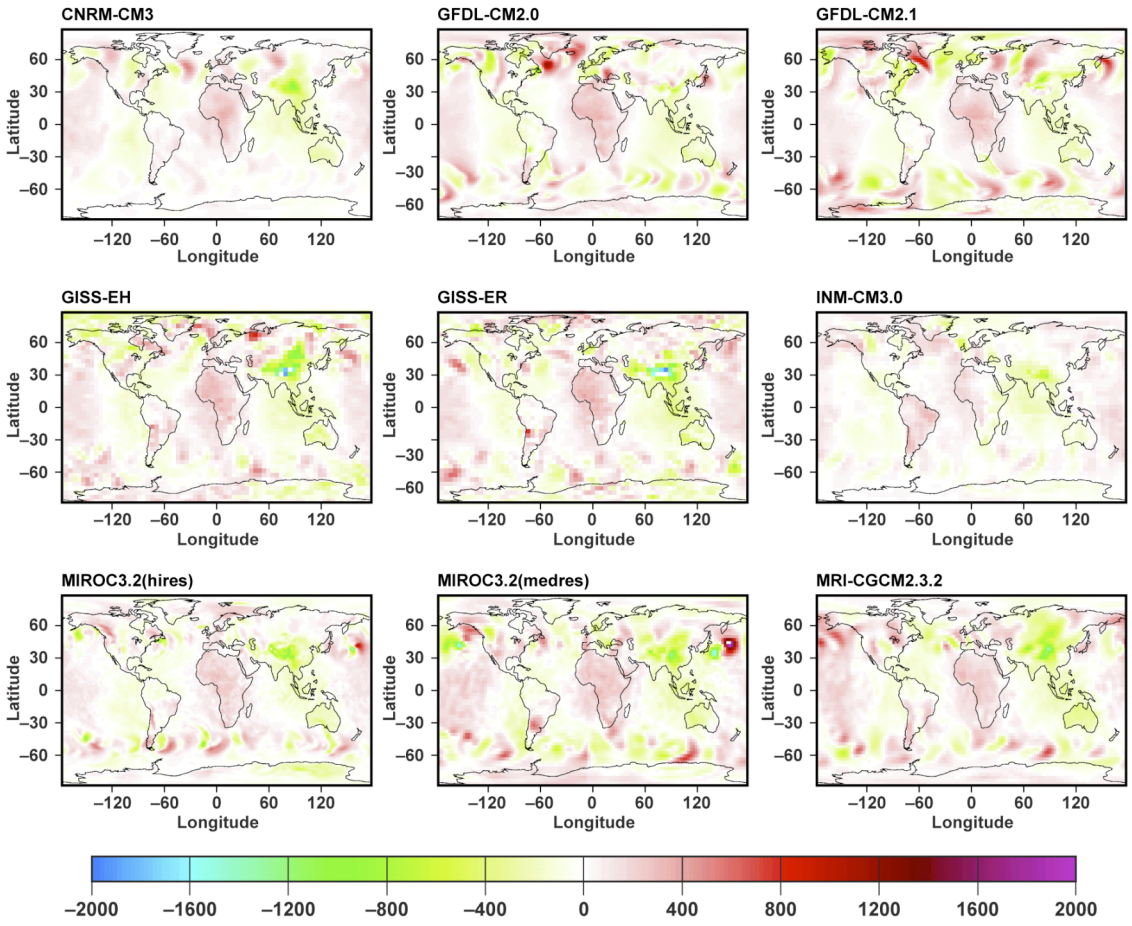

FIGURE 7: "Snapshots" of surface pressure anomalies in Pascals (relative to daily-mean surface pressure) from the end of nine CMIP3 / IPCC AR4 20th century simulations. The time of day is 10:30 AM GMT for the INM-CM3.0 and 09:00 AM GMT for all other models.